Practical design of a 4 Tesla double-tuned RF surface coil for interleaved ^{1}H and ^{23}Na MRI of rat brain

M. Alecci [a,*], S. Romanzetti [b], J. Kaffanke [b], A. Celik [b], H.P. Wegener [c], N.J. Shah [b,d]

[a] *Dipartimento di Scienze e Tecnologie Biomediche and CNR-INFM, Universita' dell'Aquila, L'Aquila, 67100, Italy*
[b] *Institute of Medicine, Research Centre Juelich, 52425 Juelich, Germany*
[c] *Central Electronic Institute, Research Centre Juelich, 52425 Juelich, Germany*
[d] *Institute of Physics, University of Dortmund, 44221 Dortmund, Germany*

Abstract

MRI is proving to be a very useful tool for sodium quantification in animal models of stroke, ischemia, and cancer. In this work, we present the practical design of a dual-frequency RF surface coil that provides ^{1}H and ^{23}Na images of the rat head at 4 T. The dual-frequency RF surface coil comprised of a large loop tuned to the ^{1}H frequency and a smaller co-planar loop tuned to the ^{23}Na frequency. The mutual coupling between the two loops was eliminated by the use of a trap circuit inserted in the smaller coil. This independent-loop design was versatile since it enabled a separate optimisation of the sensitivity and RF field distributions of the two coils. To allow for an easy extension of this simple double-tuned coil design to other frequencies (nuclei) and dimensions, we describe in detail the practical aspects of the workbench design and MRI testing using a phantom that mimics in vivo conditions. A comparison between our independent-loop, double-tuned coil and a single-tuned ^{23}Na coil of equal size obtained with a phantom matching in vivo conditions, showed a reduction of the ^{23}Na sensitivity (about 28 %) because of signal losses in the trap inductance. Typical congruent ^{1}H and ^{23}Na rat brain images showing good SNR (^{23}Na: brain 7, ventricular cerebrospinal fluid 11) and spatial resolution (^{23}Na: $1.25 \times 1.25 \times 5$ mm^3) are also reported. The in vivo SNR values obtained with this coil were comparable to, if not better than, other contemporary designs in the literature.
© 2006 Elsevier Inc. All rights reserved.

Keywords: MRI; Radio frequency surface coil; Double tuned; Proton; Sodium

1. Introduction

High static magnetic field (3 to 7 T) whole body MRI scanners are proving to be very useful for a number of applications, including quantitative proton (^{1}H) and sodium (^{23}Na) measurements in clinical studies [1]. For example, diseases of the human brain, such as stroke and brain tumours, are often associated with oedema of varying extent. Recently, using quantitative MRI mapping methods, it was found that in human brain tumours there is a significant increase in absolute water content in the vicinity of the tumour, which is not observable in conventional

T$_1$-weighted images [2]. ^{23}Na MRI with short echo times was used to quantify absolute tissue sodium concentration in patients with brain tumours showing an increase of sodium concentration in tumours relative to that in normal brain structures [3]. It seems feasible that a number of MRI centres, currently equipped with high field (3-7 T) whole body MRI scanners, should wish to carry out ^{1}H, and ^{23}Na animal studies [4] using the same scanner. To accomplish this, specially designed small-size gradient coils and RF coils are required. For example, using a 4 T whole body MRI scanner it was shown in rabbit [5] models of focal cerebral ischemia that there are changes in tissue ^{23}Na signal levels following acute ischemia, which may help to identify necrotic tissue and estimate the duration of ischemia [6]. Recent advances in ultra-high field (17.6 T)

---
* Corresponding author. Fax: +39 0862 433433.
E-mail address: marcello.alecci@univaq.it (M. Alecci).

MRI hardware have allowed the acquisition of the first [23]Na images of the mouse heart with an isotropic spatial resolution of 1 mm [7].

The previous examples show that in humans and animal models there is the need to obtain interleaved co-registered anatomical (^{1}H) and physiological ([23]Na) information which may be useful for assessing disease and effective therapeutic intervention. For this purpose, volume and/or surface RF coils tuned to the ^{1}H and [23]Na frequencies are required.

Two main design strategies of double-tuned RF coils suitable for MRI studies have been previously reported. The first makes use of two separate RF coils, one tuned to the ^{1}H frequency and the other to the [23]Na frequency [5–7]. To obtain the ^{1}H and [23]Na images in a sequential fashion, interchange of the two RF coils was required. This design is straightforward, since it avoids the problem of mutual coupling between the two RF coils, and allows a separate optimisation of the ^{1}H and [23]Na signals. However, it requires additional measurement time for coil exchange (usually a precious commodity in in vivo experiments), it introduces potential errors due to re-positioning within the MRI scanner (requires *a posteriori* co-registration of the images), and it does not allow the use of interleaved ^{1}H and [23]Na pulse sequences. The second method requires a double-tuned RF coil (^{1}H and [23]Na), which is usually made either as a volume [8–17] or surface [18–24] RF coil. This design allows interleaved ^{1}H and [23]Na images to be obtained over essentially the same volume of interest (VOI), without the need for repositioning the sample. Usually, the ^{1}H RF coil is used to obtain anatomical scout images and also for B_0 field shimming in the VOI.

A double-tuned volume RF coil is preferred when good homogeneity over the VOI is necessary and, generally, designs based on the birdcage coil have been used at low field ($\leqslant$1.5 T) [9–13] and also for 3 T [14]. For higher field MRI double tuning has been achieved using the Transverse-Electro-Magnetic (TEM) coil [15–17].

Over the past 20 years, several designs of double-tuned RF surface coils have been reported for low field applications [18–24]. In the following, only double-tuned surface coil designs capable of operation at high field (>3T) are considered. Despite their reduced RF homogeneity, with respect to the RF volume coils, double-tuned RF surface coils are preferred when the SNR of one or both nuclei is very low. A dual-frequency surface coil employing a single loop with distributed capacitance was reported at 4.1 T [25]. This approach is straightforward and gives good efficiency for both channels, but does not allow separate optimisation of the geometrical dimension of the two RF coils. A double-tuned RF surface coil that uses two mutually coupled circular loop surface coils was developed for a 7 T animal scanner [26]. This design required an adjustable spacing between the two loops, thus reducing the available volume for the sample within the MRI scanner.

In this work, we present the practical design of a dual-frequency RF surface coil that provides ^{1}H and [23]Na imag-

es of the rat brain at 4 T. It comprises of a large square loop tuned to the ^{1}H frequency and a small co-planar square loop tuned to the [23]Na frequency. The mutual coupling between the two loops is eliminated by the use of a trap circuit inserted in the smaller coil. This independent-loop design is versatile since it provides a separate optimisation of the ^{1}H and [23]Na coils sensitivity and also RF field distributions. To allow for an easy extension of this simple double-tuned coil design to other frequencies (nuclei) and dimensions, we describe in detail the practical aspects of the workbench design and MRI testing with phantoms. Typical congruent ^{1}H and [23]Na rat brain images showing good SNR and spatial resolution are also reported.

2. Double-tuned RF coil design

In this study a whole-body 4 T Unity Inova scanner (Varian, Palo Alto, CA) equipped with transmit/receive (TX/RX) ^{1}H and [23]Na imaging channels was used. A removable small bore (inner diameter 12 cm) high performance animal insert gradient (MAGNEX SGRAD 205/120/S; 400 mT/m; slew rate 2353 T/m/s; rise time 170 μs) was used for phantom and rat studies. An RF amplifier (Herley, model 4T70A) providing a maximum peak power of 7 kW (68 dBm) was used for both channels.

Fig. 1 shows the 4 T dual-frequency, dual-loop RF surface coil prototype. The coil comprises of a large square loop, tuned at the ^{1}H signal of 170.30 MHz (f_{1H}) that provides a means for accurate ^{1}H anatomical localisation and shimming of the B_0 field, and a small co-planar square loop, tuned at the [23]Na signal of 45.05 MHz (f_{23Na}) and optimised for [23]Na signal detection in the adult rat brain. The mutual coupling between the two loops is eliminated by the use of a "trap circuit" inserted in series with the
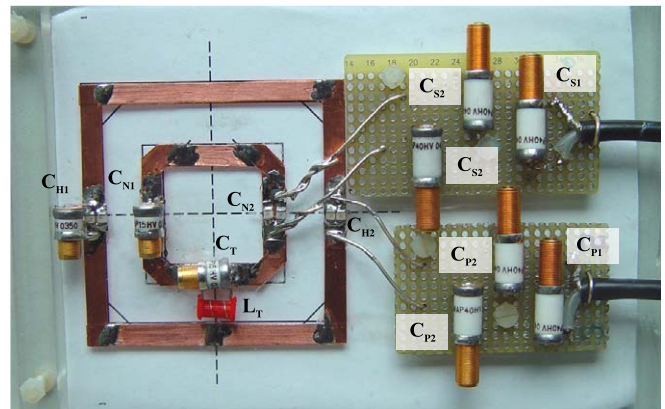

Fig. 1. The 4 T double-tuned RF coil prototype, comprising of a large square loop (65 mm) for the ^{1}H channel and a small square loop (35 mm) for the [23]Na channel. The trap circuit is inserted on the small loop ($C_T = 28$ pF + (1–15) pF trimmer; $L_T = 36.5$ nH). The matching circuits for each channel are also shown ($C_{P1} = C_{P2} = C_{P3} = (1–40)$ pF trimmer; $C_{S1} = C_{S2} = C_{S3} = 27$ pF + (1–40) pF trimmer). The tuning capacitance of the ^{1}H and [23]Na RF coil are: $C_{H1} = 3.6$ pF + 3.6 pF + (1–15) pF trimmer; $C_{H2} = 3.6$ pF + 3.6 pF; $C_{N1} = 220$ pF + 220 pF + (1–15) pF trimmer; and $C_{N2} = 220$ pF + 220 pF.

smaller coil. Our 4T RF coil design builds on previous work with 1.5 T single-coil and double-tuned RF coils [22–24].

Fig. 2 shows the lumped-parameter equivalent circuit of the double-tuned surface RF coil described in this work. Essentially, the coil can be considered as two inductively coupled series resonant circuits [27]. The primary resonant circuit is the large loop, while the secondary resonant circuit is the small loop. Without the trap circuit, the mutual coupling would produce a significant shift of the resonance frequency of each loop, with respect to the frequency of the isolated loops. The frequency shift of the ^{1}H coil is always larger than the ^{23}Na coil.

The trap circuit, inserted in series with the smaller coil, avoids mutual coupling between the ^{1}H and ^{23}Na coils. As shown in Fig. 2, the trap is a parallel resonant circuit with capacitance C_T and inductance L_T, and it allows independent and effective operation of the two channels. In fact, if the trap components are chosen according to the condition $X_{C_T} = X_{L_T}$, it acts as an open circuit at f_{1H} and the frequency shift due to the mutual coupling between primary and secondary coils is practically eliminated. The achievement of this condition requires fine-tuning of the trap capacitance. At frequencies below and above f_{1H}, the trap circuit behaves as an equivalent inductive or capacitive load, respectively, and the small loop coil presents two resonant modes with frequencies f_{LF} and f_{HF} ($f_{LF} < f_{1H} < f_{HF}$) given by:

$$f_{LF} = 1/2\pi\sqrt{(L_T + L_S) \cdot C_S}, \tag{1}$$

$$f_{HF} = 1/2\pi\sqrt{L_S \cdot \left(\frac{C_S \cdot C_T}{C_S + C_T}\right)}. \tag{2}$$

As shown in Eq. (1), the appropriate selection of the total series inductance ($L_T + L_S$) and capacitance C_S in the secondary circuit allows the tuning of f_{LF} to the desired ^{23}Na frequency. As shown in earlier work on single-loop double-tuned RF coils [23], the optimisation of the ^{23}Na sensitivity requires $L_T \ll L_S$. However, for small size loops

Fig. 2. Equivalent lumped-parameter circuit of the 4 T double-tuned RF surface coil. The matching capacitances for the ^{1}H channel comprised trimmer capacitors only ($C_{P1} = C_{P2} = C_{P3} = (1–40)$ pF) while the ^{23}Na matching capacitances required a trimmer capacitor in parallel with a chip capacitor ($C_{S1} = C_{S2} = C_{S3} = 27$ pF + (1–40) pF trimmer). The equivalent tuning capacitance for the ^{1}H channel (C_P) comprised the series connection of C_{H1} and C_{H2} (see Fig. 1). The equivalent tuning capacitance for the ^{23}Na channel (C_S) comprised the series connection of C_{N1} and C_{N2} (see Fig. 1). The trap capacitance comprised a chip capacitor in parallel with a trimmer capacitor ($C_T = 27$ pF + (1–40) pF trimmer).

this condition is difficult to fulfil and some degree of sensitivity reduction in the ^{23}Na channel, with respect to the isolated single-tuned coil, is unavoidable. As shown in Eq. (2), if we assume that $C_S \gg C_T$ then the high frequency mode f_{HF} is only determined by L_S and C_T.

It is worth noting that the insertion of the trap circuit in the ^{1}H coil (high gamma nucleus) instead of the ^{23}Na coil (low gamma nucleus) is, unfortunately, not feasible. This is a consequence of the role played by the trap circuit and the large frequency separation between the ^{1}H and ^{23}Na nuclei ($\Delta f = 125$ MHz). In fact, when the trap is inserted in the ^{23}Na coil and fine tuned to the ^{1}H frequency (f_{1H}) it acts as an open circuit, thus eliminating mutual coupling. As discussed above, at frequencies below and above f_{1H} the trap circuit behaves as an equivalent inductive or capacitive load, respectively, and the ^{23}Na coil presents two resonant modes positioned around the trap frequency ($f_{LF} < f_{1H} < f_{HF}$). In this condition the lower mode f_{LF} can always be tuned to the ^{23}Na frequency by increasing the capacitance C_S (see Eq. (1)), while the higher mode f_{HF} is not used. Suppose now that the trap is inserted in the large ^{1}H coil and fine tuned to the ^{23}Na frequency to eliminate mutual coupling. In this configuration, the lower and higher modes would be centred around f_{23Na}, and the only way to tune the large coil to f_{1H} would be to increase f_{HF}. As shown in Eq. (2) this can be achieved only by reducing the equivalent capacitance given by the series connection of C_S and C_T. However, because of the very large frequency separation between the ^{1}H and ^{23}Na nuclei this is not feasible, since a very small equivalent capacitance would be required. Finally, it is useful to note that when designing double tuned coils for nuclei with relatively close resonant frequencies (e.g. ^{1}H and ^{19}F) the positioning of the trap in the higher gamma nucleus could be feasible, thus completely eliminating signal losses at the lower gamma nucleus.

Considering the large frequency separation (125 MHz) of the ^{1}H and ^{23}Na channels, the use of a single broad-band matching circuit suitable for a single coil operated at both frequencies does not seem to be feasible. Moreover, the need for retuning from the ^{1}H to the ^{23}Na channel would introduce an additional time penalty which is inconvenient for in vivo studies. The idea of using a single volume RF coil and two separate and removable tuning/matching circuits has been recently used in the context of fluorine-proton double resonance imaging [28]. However, this design also requires an additional switching time and it does not allow separate optimisation of the spatial distribution of the RF fields of the lower and higher modes.

3. Practical design and testing

The resonant frequency, the reflection coefficient, S_{11}, and the quality factor, Q, of the 4 T double-tuned RF coil prototype were measured with a network analyser (Rohde &Schwarz, ZVR). The accurate set-up of the coil requires a number of careful experimental steps making the procedure worth describing in some detail.
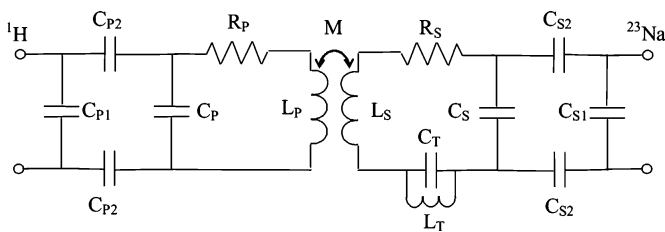
(1) *Geometrical layout of the RF coils*. The large (external size 65 mm × 65 mm) and the small (external size 35 mm × 35 mm) loops, see Fig. 1, were made of adhesive copper strips (width 5 mm, thickness 80 μm). These dimensions were chosen to allow full anatomical coverage (^{1}H) and good sensitivity (^{23}Na) in the brain of adult rats, with a body weight of about 250 g. The measured inductances of the large and small coils were 128 and 47 nH, respectively. The estimated mutual inductance, M, between the large and small loops is 165 nH [29]. A rectangular acrylic substrate (110 mm × 160 mm × 3 mm) was as a base for the copper strips and the matching circuits of the ^{1}H and ^{23}Na channels. Two standard 50 Ω coaxial cables (RG58) were used to drive each channel of the RF coil.

(2) *Design of the matching circuits*. The matching circuit, see Fig. 2, was made using a balanced capacitive configuration [30] for both channels. The ^{1}H matching required three trimmer capacitors (NMAP40HV0408; Voltronics, USA) of value 1–40 pF (see Fig. 1). The matching network was mounted on a PCB board and a preliminary calibration of the matching circuit was made by connecting a 50 Ω load resistor to the matching network. The measured S_{11} response showed a pronounced dip with a very large bandwidth (about 200 MHz). The centre frequency of the dip could be varied through a wide range (40–250 MHz) by adjusting, in a balanced manner, the two C_{P2} trimmers (see Fig. 2). The C_{P1} trimmer was used to adjust the degree of matching (at least −20 dB) by measuring the S_{11} parameter. After connecting the matching network to the large ^{1}H RF coil, a reduction of its tuning frequency by about 10 MHz was observed as compared to the value measured with a small pick-up loop positioned at about 2 cm from the RF coil. This indicates that the ^{1}H coil needs to be carefully retuned once the matching network is connected. A similar design and calibration procedure was adopted for the matching network of the ^{23}Na channel. However, to decrease the matching range to about 45 MHz, a 27 pF chip capacitor (ATC, USA) was connected in parallel with each of the three trimmer (1–40 pF) capacitors C_{S1}, C_{S2}, and C_{S3} (NMAP40HV0408; Voltronics, USA) of the matching network. After connecting the matching network, the frequency of the ^{23}Na RF surface coil was reduced by about 0.5 MHz only as compared to the value measured with the small pick-up loop positioned at about 1 cm from

the coil. A fine-tuning of the small ^{23}Na RF coil was also required once the matching network had been connected.

(3) *Workbench and MRI testing of the ^{1}H coil alone (^{23}Na coil open)*. The adhesive copper tape layout of the ^{1}H and ^{23}Na loops was positioned on the acrylic substrate. Two cuts (width about 2 mm) one each on opposite sides of each loop were made. No capacitors were connected to the small ^{23}Na loop. The large ^{1}H loop was tuned by connecting two 3.6 pF chip capacitors (ATC, USA) across the gaps in the matching and tuning sides of the coil, respectively. To allow a fine-tuning of the large RF coil, a trimmer (1–15 pF) capacitor (NMAP15HV0350; Voltronics, USA) was also connected on the tuning side, see Fig. 1. The position of these tuning capacitors corresponds to the virtual ground of the ^{1}H RF coil. After connection of the matching circuit (see point 2), the ^{1}H coil was fine tuned/matched in the presence of a cylindrical phantom (diameter about 45 mm) containing 37 ml of 45 mM saline solution. The size and composition of this phantom was chosen to mimic the average sodium concentration of the brain [31], and also to mimic typical adult rat loading of the RF coil. The RF coil was then placed in the MRI scanner and tested for the 90° flip angle calibration, see Table 1, and standard 3D gradient echo imaging.

(4) *Workbench and MRI testing of the ^{23}Na coil alone (^{1}H coil open)*. To avoid inductive coupling between the ^{1}H and ^{23}Na coils, a small cut was made at one side of the large RF coil to detune it totally. The small ^{23}Na loop was tuned by connecting two 220 pF chip capacitors (ATC, USA) across the gaps in the matching and tuning sides of the coil, respectively. To allow a fine-tuning of the small RF coil, a trimmer (1–15 pF) capacitor was also connected on the tuning side. After connection of the matching circuit (see point 2), the ^{23}Na RF coil was fine tuned/matched in the presence of the cylindrical phantom. The RF coil was placed in the MRI scanner and tested, see Table 1.

(5) *Workbench and MRI testing of the ^{23}Na and ^{1}H coil without trap*. To measure the coupling between the ^{1}H and ^{23}Na RF coils, the cut on the large coil was soldered and the S_{11} response showed two resonant frequencies (45.01 and 173.20 MHz). These two modes were due to the mutual inductive coupling between the ^{1}H and ^{23}Na RF coils. We observe that the coupling produces a small frequency shift for the ^{23}Na coil (−0.05 MHz) and a large

Table 1
RF parameters of the double-tuned RF surface coil for 4 T MRI

Coil design	f_0 (MHz)	S_{11} (dB)	$Q \pm 3$	90° flip angle (μs) @ 37 dBm
^{23}Na coil alone	45.06	−36	80	188
^{1}H coil alone	170.40	−21	76	450
^{23}Na and ^{1}H coil with trap	45.03	−41	65	240
	170.40	−36	81	475
^{23}Na and ^{1}H coil with trap (in vivo)	45.00	−38	64	230
	170.17	−33	72	350

The data were acquired in the presence of a cylindrical phantom (diameter 45 mm, volume about 37 ml) containing 45 mM of Na, except for the last row data where a rat (257 g) was positioned in the supine with the head centred in the RF coil. The RF amplifier provided a maximum peak power of 7 kW (68 dBm). The scanner TX frequency was set to 45.036 MHz (sodium) or 170.259 MHz (proton) for all the measurements.

shift for the ^{1}H coil (2.8 MHz), with respect to the RF coils when isolated from each other. The large frequency shift of the ^{1}H coil makes its use impractical for proton imaging, since its sensitivity at the ^{1}H operating frequency (170.259 MHz) is greatly reduced. The degree of coupling depends on the relative size and position of the two coils, and also on their respective quality factors [27].

(6) *Workbench calibration of the trap circuit*. The inductive coupling was eliminated by inserting, in series with the small coil, a trap circuit made of a 36.5 nH solenoid (3 turns, diameter 5 mm; Memec GmbH, Germany) connected in parallel with a 28 pF chip capacitor. To allow fine-tuning of the trap circuit a trimmer (1–15 pF) capacitor was inserted in the trap circuit, see Fig. 1. The insertion of the trap inductance decreases the lower resonant frequency of the small ^{23}Na loop (see Eq. (1)) and to retune the coil to 45.05 MHz an additional chip capacitor (100 pF) was connected across the gaps in the matching and tuning sides of the coil. In this condition the S_{11}, measured from the ^{1}H channel, showed the presence of three resonances, see Fig. 3A. The lower and higher frequencies, f_{LF} and f_{HF}, are the resonant modes of the small loop coil in the presence of the trap circuit, given by Eqs. (1) and (2). The intermediate frequency, f_{1H}, is the resonance of the large coil and it can be set to 170.30 MHz by a proper adjustment of the trap capacitance. The S_{11} measured from the ^{23}Na channel is reported in Fig. 3B where it can be seen that only the lower frequency, f_{LF}, is well matched.

(7) *MRI testing of the double-tuned RF coil with a phantom*. After fine-tuning of the trap circuit, the double-tuned RF coil was used for ^{1}H and ^{23}Na MRI testing. The measured RF parameters and the calibrated 90° flip angle values are reported in Table 1. It can be seen that the presence of the trap circuit is very effective in eliminating the coupling between the ^{1}H and ^{23}Na channels, since the resonant frequencies are practically identical to the one measured for

each RF coil when isolated (see Table 1). However, from the 90° flip angle data of Table 1 obtained with the phantom, it can be seen that the single-tuned ^{23}Na coil requires a flip angle pulse length of 188 μs, while the double-tuned coil requires a flip angle pulse length of 240 μs. This increased pulse length (about 28%) is determined by additional losses in the trap inductance. The results of Table 1, show that the 90° flip angle required for the single-tuned ^{1}H coil (450 μs) is practically the same as the one measured with the double-tuned coil (475 μs). Of course, the increased 90° flip angle measured in the presence of the phantom with our double-tuned design is a drawback in terms of coil sensitivity for the ^{23}Na channel. However the capability to independently adjust the size of the ^{1}H and ^{23}Na coils is very convenient because it allows a closer conformity of the coil geometries to the rat head, providing a further sensitivity improvement, and increased versatility in the experimental set-up. Fitzsimmons et al. [23] reported the design of a transformer-coupled, double-resonant probe design for a 2 T imager. As compared to a single-tuned RF coil of identical size, this design showed an SNR practically unchanged for the lower frequency (34 MHz), while the SNR of the higher frequency (85 MHz) decreases by 50% since it corresponds to a counter-current mode [23]. We are unable to estimate the SNR performances of the Fitzsimmons et al. [23] design when operated at higher field strengths (>2T). However, it is worth noting that the double-tuned coil reported in [23] is based on a single-coil design, and it does not allow separate optimisation of the RF field spatial distributions of the lower and higher modes. From the data given in Table 1 we observe that, for the double-tuned coil in the presence of the phantom, the loading of the ^{23}Na channel ($Q = 65$, 90° flip angle = 240 μs) is practically the same as the one measured with the rat head ($Q = 64$, 90° flip angle = 230 μs). However, the loading of the ^{1}H channel in the presence of the phantom ($Q = 81$, 90° flip angle = 475 μs) is smaller as compared to that measured with the rat head ($Q = 72$, 90° flip angle = 350 μs).

4. Phantom and in vivo ^{1}H and ^{23}Na MRI

Following shimming, proton and sodium images of a phantom and rat brain ($n = 3$, average body weight of 250 g) were obtained with a 3D GRE pulse sequence. All in vivo procedures followed the guidelines of the local committee for animal care of the Institute of Medicine (Research Centre Juelich). The signal-to-noise-ratio (SNR) of the magnitude images was calculated as SNR $= 1.25 \times I_S/I_N$, where I_S and I_N are the average signal amplitude in a central ROI and the average noise level in a background ROI [32], respectively.

Fig. 4 shows the congruent proton (A–B) and sodium (C–D) GRE images of the phantom in the axial and coronal planes. The ^{1}H images were collected with a FOV=$64 \times 64 \times 64$ mm^3 and an acquisition matrix of $128 \times 128 \times 64$ which resulted in an acquired spatial resolu-
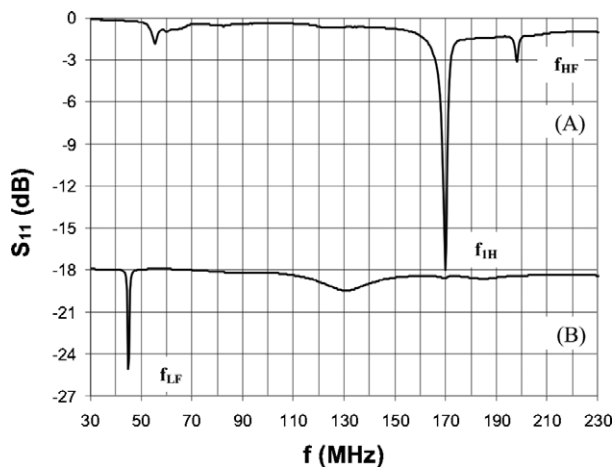

Fig. 3. The S_{11} response of the double-tuned RF coil prototype as measured from the ^{1}H (A) or the ^{23}Na (B) channel. The RF coil was loaded with a cylindrical phantom (diameter 45 mm, volume about 37 ml) containing 45 mM of Na. For ease of visualisation the reference S_{11} value of the ^{23}Na channel was shifted by −18 dB.
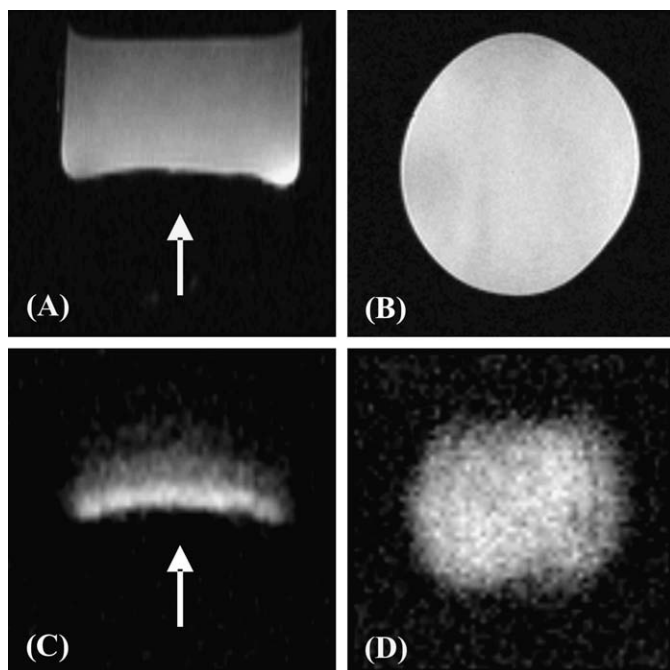
Fig. 4. Congruent 3D GRE ^{1}H axial (A), ^{1}H coronal (B), ^{23}Na axial (C), and ^{23}Na coronal (D) images obtained with a cylindrical phantom (diameter about 45 mm, volume 37 ml) containing 45 mM of sodium. The arrows show the position chosen to obtain the ^{1}H and ^{23}Na MRI signal profiles of Fig. 5.

tion of $0.5 \times 0.5 \times 1$ mm^3. The acquisition parameters were: TR = 20 ms, TE = 5 ms, flip angle $\alpha = 20°$, non-selective rectangular pulse of length 200 µs, NEX = 2, bandwidth 100 kHz, and a total acquisition time of about 5 min. The ^{23}Na images were collected with a FOV = $64 \times 64 \times 64$ mm^3 and an acquisition matrix of $64 \times 64 \times 8$. The spatial resolution of the acquisition was $1 \times 1 \times 8$ mm^3. Before transformation of the acquired data to the image space, zero filling to $64 \times 64 \times 32$ was applied. Furthermore, for final display the images were interpolated to a $64 \times 64 \times 64$ matrix. The acquisition parameters were as follows: TR = 20 ms, TE = 2.9 ms, NEX = 200, non-selective rectangular pulse of length 200 µs, bandwidth = 6.4 kHz, and a total acquisition time of about 43 min. To allow for comparison of phantom data with the in vivo data, the flip angle was $\alpha = 45°$ (Ernst angle) assuming a T$_1$ of 60 ms for ^{23}Na at 4 T [5,33].

For the ^{1}H and ^{23}Na coronal slices (see Fig. 4), the measured SNR was 29 and 8, respectively. The ^{23}Na phantom image shows a good spatial resolution and SNR in the central ROI. It is worth noting that the diameter of the phantom is larger than the size of the ^{23}Na coil and the B_0 field is directed along the inferior/superior direction. This explains the signal drop out observed at the edges of the phantom evident in the ^{23}Na coronal image of Fig. 4D, where near the inferior/superior edges the B_0 and B_1 field are directed along the same direction. This signal drop out is not observed in the ^{1}H coronal image of Fig. 4B because the diameter of the phantom being smaller than the diameter of the ^{1}H coil. The image distortion observed in Fig. 4B

is probably due to a small asymmetry in the shape of the cylindrical phantom and some gradient non-linearity. The axial ^{1}H and ^{23}Na slices of Fig. 4 show a typical sensitivity decrease along the posterior/anterior direction. The normalised MRI signal decay of the axial ^{1}H and ^{23}Na images along the posterior/anterior direction is shown in Fig. 5. The MRI sensitivity depth (50% of maximum signal) scales approximately with the RF coil size and the measured values were about 45 and 15 mm for the ^{1}H and ^{23}Na RF coils, respectively.

Fig. 6 shows congruent ^{1}H (top) and ^{23}Na (bottom) axial rat head images going from superior (A) to inferior (F). The gap between the slices is 4 mm, and the slice thickness is 0.5 and 0.6 mm for the ^{1}H and ^{23}Na, respectively. The in vivo ^{1}H images were collected with a FOV = $64 \times 64 \times 64$ mm^3 and acquisition matrix of $128 \times 128 \times 64$. The in vivo ^{1}H acquisition parameters were: TR = 20 ms, TE = 5 ms, flip angle $\alpha = 20°$, NEX = 1, bandwidth = 100 kHz, and a total acquisition time of 3 min. The in vivo ^{23}Na axial (Fig. 6) and coronal (Fig. 7) images were collected with a FOV = $40 \times 40 \times 80$ mm^3 and acquisition matrix of $32 \times 32 \times 16$, giving a voxel volume of 8 µl ($1.25 \times 1.25 \times 5$ mm^3). As for the phantom images of Fig. 4, before transformation of the acquired data to the image space, zero filling to $32 \times 32 \times 32$ was applied. Furthermore, for final display the images were interpolated to a $64 \times 64 \times 64$ matrix. The acquisition parameters were as follows: TR = 20 ms, TE = 2.9 ms, NEX = 200, non-selective rectangular pulse of length 200 µs, bandwidth = 6.4 kHz, and total acquisition time of 35 min. The flip angle was $\alpha = 45°$ (Ernst angle) assuming a T$_1$ of 60 ms for ^{23}Na at 4 T [5].

The axial ^{23}Na head rat images of Fig. 6 show a good SNR, spatial resolution and correspondence to anatomical details. For example, from the axial slices of Fig. 6B, the average SNR in the rat brain for the ^{1}H and ^{23}Na images
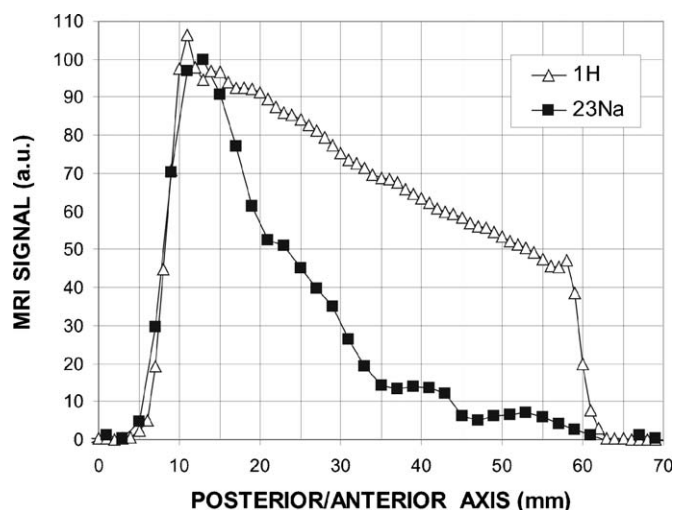

Fig. 5. The normalised ^{1}H and ^{23}Na MRI signal decay along the posterior/anterior direction obtained from the central line (see arrows in Fig. 4) of the 3D GRE axial images of Fig. 4A and C.
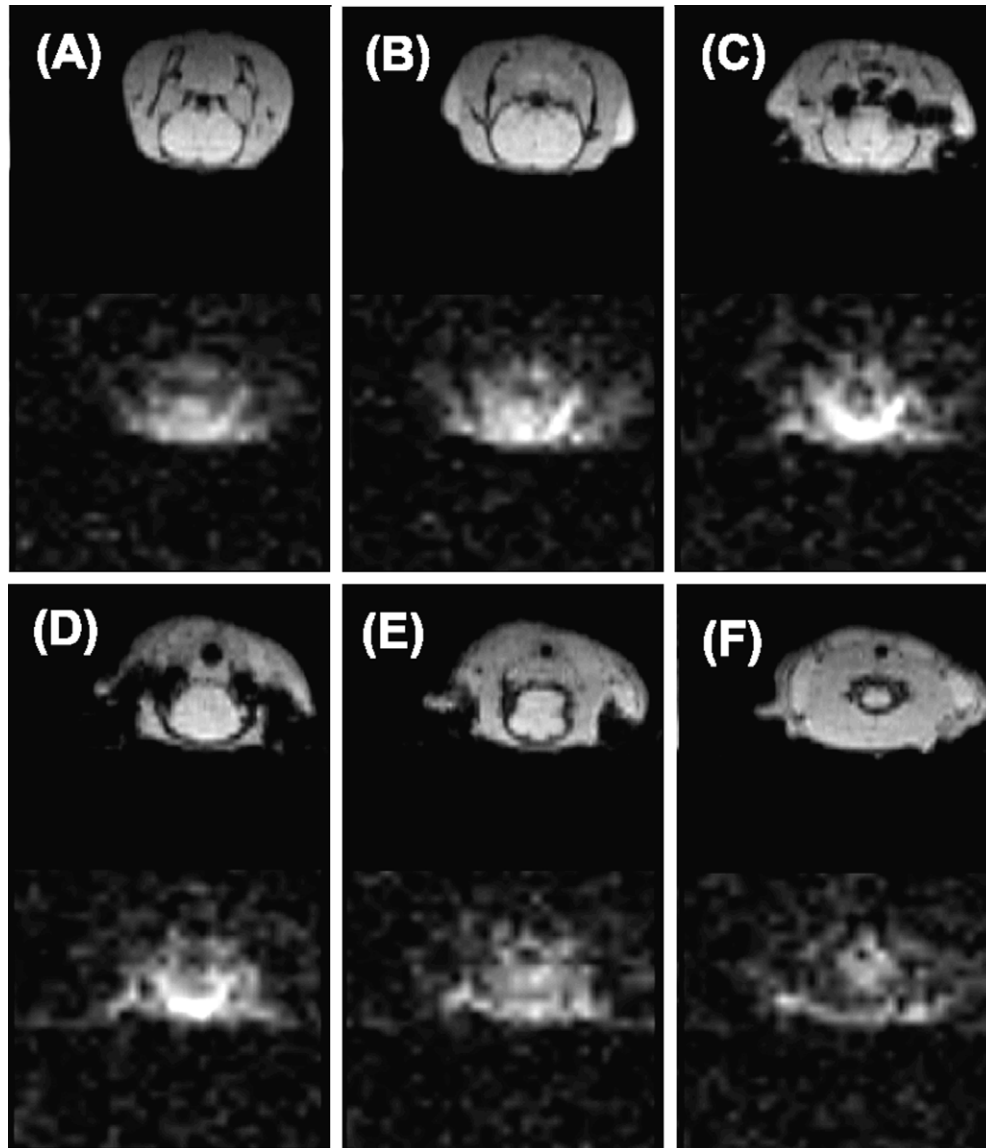
Fig. 6. Congruent 3D GRE ^{1}H (top) and ^{23}Na (bottom) axial rat brain images from the superior (A) to the inferior (F) end. The gap between slices is 4 mm, and the slice thickness is 0.5 and 0.6 mm for the ^{1}H and ^{23}Na, respectively.

was, respectively, about 25 and 7. Fig. 6D shows a hyper intense ^{23}Na region (SNR of about 11), corresponding to the ventricular cerebrospinal fluid (CSF) space, which has a higher concentration of ^{23}Na and longer T_2 than ^{23}Na in the brain tissues. From Fig. 6F, the ^{23}Na signal arising from the spinal cord can be detected. The congruent ^{1}H and ^{23}Na coronal brain images of Fig. 7 show good SNR and spatial resolution. It is worth noting that an higher SNR (brain 18; CSF 40) has been reported in the rabbit using two separate ^{1}H and ^{23}Na RF coils, asymmetric k-space readout and reduced sampling in the phase encode directions, and Gaussian filtering [5]. Since the SNR is proportional to the pixel volume, the higher SNR observed in the rabbit is due to the larger image pixel volume (27 µl) as compared to that achieved in the rat (8 µl) in the present work. For a comparable voxel size, our coil would give an SNR of 23 for the brain and 37 for CSF. Further

improvements can be expected for an asymmetric k-space readout with reduced sampling in the phase encode directions, and Gaussian filtering. Taken together, this indicates that the performance of the design presented here is at least as good as, if not better than, rival designs in the literature.

5. Conclusions

In summary, we have reported the design and testing of a simple dual-frequency surface RF coil providing proton and sodium images of rat brain at 4 T. The advantages of this coil design are: minimal space requirement for the coil, since the ^{1}H and ^{23}Na loops are co-planar; ease of construction and modest cost; independent driving of the ^{1}H and ^{23}Na channels; automatic co-registration of the ^{1}H and ^{23}Na images; and good SNR and spatial resolution. The main disadvantages are: limited RF homogeneity of
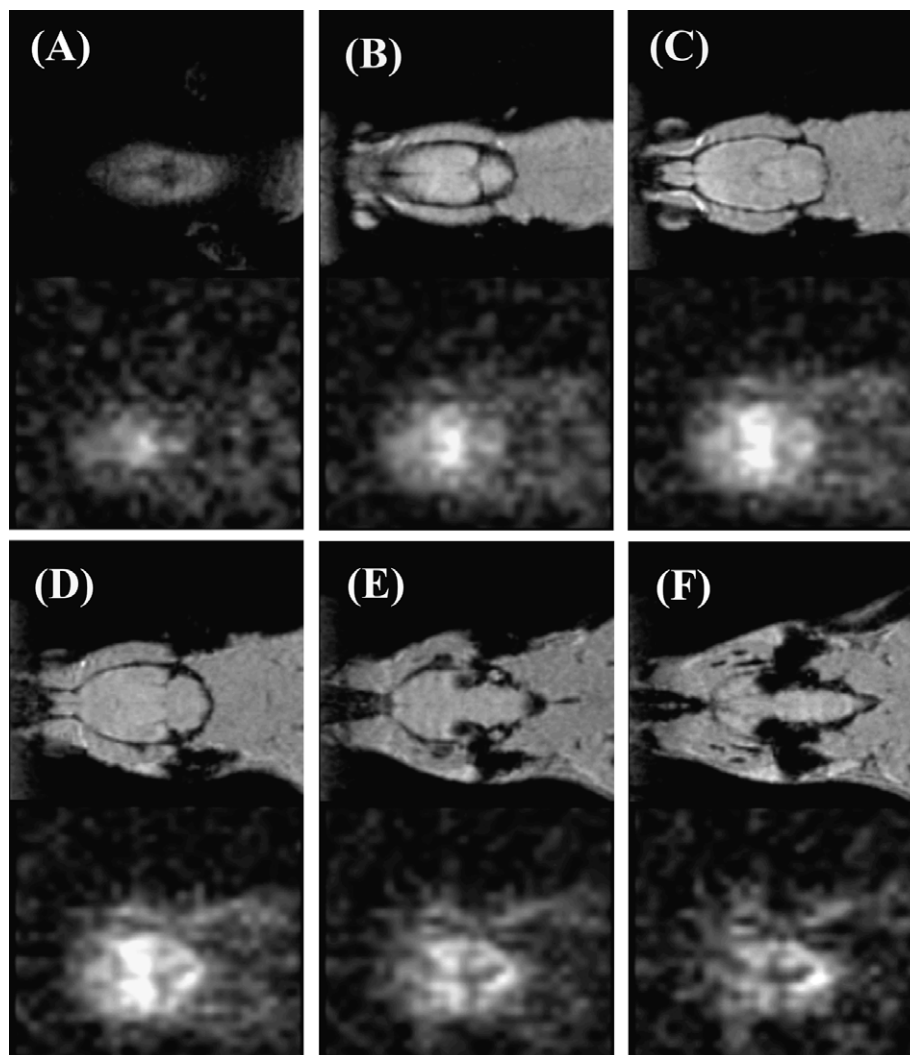
Fig. 7. Congruent 3D GRE ^{1}H (top) and ^{23}Na (bottom) coronal rat brain images from the posterior (A) to the anterior (F) end. The gap between slices is 2 mm, and the slice thickness is 0.5 and 0.6 mm for the ^{1}H and ^{23}Na, respectively.

the ^{23}Na channel along the anterior/posterior direction (about 15 mm); and a reduction of the ^{23}Na sensitivity (about 28 %) because of the trap circuit, as compared to a single tuned ^{23}Na coil of equal size. The axial and coronal ^{23}Na density-weighted images of the rat brain, obtained in about 35 min, show a reasonable spatial resolution and SNR. From the axial images, a higher ^{23}Na concentration in the ventricular CSF space was observed. We expect the use of printed circuit board technology for the manufacture of the ^{1}H and ^{23}Na coils, and closer conformity of the coil geometries to the rat head, should provide further improvements to sensitivity. This simple and cheap dual-frequency surface RF coil design should be a useful tool for ^{23}Na quantification of animal models using high field ($\geqslant$4T) MRI.

Acknowledgment

References

[1] K. Ugurbil, G. Adriany, P. Andersen, W. Chen, M. Garwood, R. Gruetter, P.G. Henry, S.G. Kim, H. Lieu, I. Tkac, T. Vaughan, P.F. Van De Moortele, E. Yacoub, X.H. Zhu, Ultrahigh field magnetic resonance imaging and spectroscopy, Magn. Reson. Imaging 21 (2003) 1263–1281.

[2] H. Neeb, J. Smyej, K. Zilles, N.J. Shah, A new method for fast quantitative mapping of absolute water content in vivo, Proc. Intl. Soc. Magn. Reson. Med. 13 (2005) 2372.

[3] R. Ouwerkerk, K.B. Bleich, J.S. Gillen, M.G. Pomper, P.A. Bottomley, Tissue sodium concentration in human brain tumours as measured with ^{23}Na MR imaging, Radiology 227 (2003) 529–537.

[4] P. Marzola, F. Osculati, A. Sbarbati, High field MRI in preclinical research, Eur. J. Radiol. 48 (2003) 165–170.

[5] R. Bartha, T.Y. Lee, M.J. Hogan, S. Hughes, E. Barberi, N. Rajakumar, R.S. Menon, Sodium T2*-weighted MR imaging of acute focal cerebral ischemia in rabbits, Magn. Reson. Imaging 22 (2004) 983–991.

[6] Y. Wang, W. Hu, A.D. Perez-Trepichio, T.C. Ng, A.J. Furlan, A.W. Majors, S.C. Jones, Brain tissue sodium is a ticking clock telling time after arterial occlusion in rat focal cerebral ischemia, Stroke 31 (2000) 1386–1391.

[7] T. Neuberger, A. Greiser, M. Nahrendorf, P.M. Jakob, C. Faber, A.G. Webb, ^{23}Na microscopy of the mouse heart in vivo using density-weighted chemical shift imaging, MAGMA 17 (2004) 196–200.

[8] J. Tropp, S. Sugiura, A dual-tuned probe and multiband receiver front end for X-nucleus spectroscopy with proton scout imaging in vivo, Magn. Reson. Med. 11 (1989) 405–412.

[9] A.R. Rath, Design and performance of a double-tuned birdcage coil, J. Magn. Reson. 89 (1990) 41–50.

[10] D.F. Lu, P.M. Joseph, A technique of double-resonant operation of ^{19}F and ^{1}H quadrature birdcage coils, Magn. Reson. Med. 19 (1991) 180–185.

[11] J.R. Fitzsimmons, B.L. Beck, H.R. Brooker, Double resonant quadrature birdcage, Magn. Reson. Med. 30 (1993) 107–114.

[12] G.X. Shen, F.E. Boada, K.R. Thulborn, Dual-frequency, dual-quadrature, birdcage RF coil design with identical B_1 pattern for sodium and proton imaging of the human brain at 1.5 T, Magn. Reson. Med. 38 (1997) 717–725.

[13] G.B. Matson, P. Vermathen, T.C. Hill, A practical double-tuned ^{1}H/^{31}P quadrature birdcage head coil optimized for ^{31}P operation, Magn. Reson. Med. 42 (1999) 173–182.

[14] G.X. Shen, J.F. Wu, F.E. Boada, K.R. Thulborn, Experimentally verified, theoretical design of dual-tuned, low-pass birdcage radiofrequency resonators for magnetic resonance imaging and magnetic resonance spectroscopy of human brain at 3.0 Tesla, Magn. Reson. Med. 41 (1999) 268–275.

[15] J.T. Vaughan, H.P. Hetherington, J.O. Otu, J.W. Pan, G.M. Pohost, High frequency volume coils for clinical NMR imaging and spectroscopy, Magn. Reson. Med. 32 (1994) 206–218.

[16] X. Zhang, X. Zhu, H. Qiao, H. Liu, J.T. Vaughan, K. Ugurbil, W. Chen, A circular-polarized double-tuned (31P and 1H) TEM coil for human head MRI/MRS at 7T, Proc. Intl. Soc. Mag. Reson. Med. 11 (2003) 423.

[17] A. Vitacolonna, G. Placidi, A. Sotgiu, P. Jezzard, M. Alecci, Theory of double tuned TEM resonators and workbench validation in a frequency range of 100-350 MHz, Proc. Intl. Soc. Magn. Reson. Med. 13 (2005) 2423.

[18] M.D. Schnall, V.H. Subramanian, J.S. Leigh Jr., B. Chance, A new double-tuned probe for concurrent ^{1}H and ^{31}P NMR, J. Magn. Reson. 65 (1985) 122–129.

[19] W.M. Chew, M.E. Moseley, M.C. Nishimura, T. Hashimoto, L.H. Pitts, T.L. James, A novel double-surface coil approach to phospho-rus-31 spectroscopy: a study of hemispheric brain injury in the rat, Magn. Reson. Med. 2 (1985) 567–575.

[20] M.O. Leach, A. Hind, R. Sauter, H. Requardt, H. Weber, The design and use of a dual-frequency surface coil providing proton images for improved localization in ^{31}P spectroscopy of small lesions, Med. Phys. 13 (1986) 510–513.

[21] P. Styles, Passive electrical isolation of double coil probes for localized spectroscopy and imaging, NMR Biomed. 1 (1988) 61–66.

[22] J.R. Fitzsimmons, H.R. Brooker, B. Beck, A transformer-coupled double-resonant probe for NMR imaging and spectroscopy, Magn. Reson. Med. 5 (1987) 471–477.

[23] J.R. Fitzsimmons, H.R. Brooker, B. Beck, A comparison of double-tuned surface coils, Magn. Reson. Med. 10 (1989) 302–309.

[24] M. Schnall, Probes tuned to multiple frequencies for *in vivo* NMR, NMR Basic Principles and Progress 26 (1992) 33–63.

[25] J.T. Vaughan, P. Roeschmann, J.W. Pan, H.P. Hetherington, B.L.W. Chapman, P. Noa, J. Vermeulen, G.M. Pohost, A double resonant surface coil for 4.1 T whole body NMR, Proc. Intl. Soc. Magn. Reson. Med. 6 (1998) 722.

[26] V. Volotovskyy, B. Tomanek, I. Corbin, R. Buist, U.I. Tuor, J. Peeling, Doubly tunable double ring surface coil, Concepts Magn. Reson. B 17B (2002) 11–16.

[27] F.E. Terman, Radio Engineering, McGraw-Hill, New York, 1937.

[28] A. Modica, D.J. Lurie, M. Alecci, Sequential, co-registered fluorine and proton field-cycled Overhauser imaging at a detection field of 59 mT, Phys. Med. Biol. 51 (2006) N39–N45.

[29] F.W. Grover, Inductance Calculations: Working Formulas and Tables, Dover, New York, 1962, p. 66-87.

[30] C.N. Chen, D.I. Hoult, Biomedical Magnetic Resonance Technology, IOP Publishing, Bristol, UK, 1989.

[31] S. Romanzetti, J. Kaffanke, M. Halse, J. Rioux, T. Dierkes, B. Balcom, N.J. Shah, In vivo sodium imaging of the human brain using conical-SPRITE, Proc. Intl. Soc. Magn. Reson. Med. 13 (2005) 2567.

[32] W.A. Edelstein, P.A. Bottomley, L.M. Pfeifer, A signal-to-noise calibration procedure for NMR imaging systems, Med. Phys. 11 (1984) 180–185.

[33] T.B. Parrish, D.S. Fieno, S.W. Fitzgerald, R.M. Judd, Theoretical basis for sodium and potassium MRI of the human heart at 1.5 T, Magn. Reson. Med. 38 (1997) 653–661.